FY2020 Progress Report To:

the

Japan Aerospace Exploration Agency

Validation of GCOM-W1 products using global water and energy balance monitoring at the Murray-Darling Basin in Australia

---

Specification No: **JX-PSPC-524352**; Contract No: **20RT000196**

Investigators: Jeffrey Walker (ER2GWF106), Jason Beringer, Christoph Rüdiger, Ying Gao

Contributors: Mei Sun Yee, Kiri Mason

March 2021

MONASH University Engineering

Executive Summary

This report presents the research activities and research outcomes for the project 'Validation of GCOM-W1 products using global water and energy balance monitoring at the Murray-Darling Basin in Australia' during JFY 2020. One of the main research activities aimed to continue operating the JAXA flux tower within the core validation site located in Yanco, New South Wales, Australia. This provides spatially distributed soil moisture data from across an AMSR2 sized footprint. It was proposed that during JFY 2020, this project would make significant independent and collaborative contributions to:

i) Continuing the validation of the AMSR2 soil moisture product against in-situ observations.

ii) Intercomparing the AMSR2 soil moisture product with complimentary satellite soil moisture products from other missions, such as SMAP.

iii) Calculating the satellite based crop coefficient/plant factor Kc using AMSR2 soil moisture product and MODIS vegetation indices.

As the AMSR2 VWC research product will be available in early 2021, the validation of VWC research product will be done in JFY 2021.

Similar to previous years, for JFY 2019 to JFY 2020, AMSR2 L3 product (10km & 25km) still underestimates the soil moisture when compared with the tower measurements and representative stations, especially during wet season.

For 2019-2020, AMSR2 L3 product (10km & 25km) still underestimates the soil moisture when compared with the tower measurements and representative stations, especially during wet season (soil moisture ranges from 0.1-0.4 m^3/m^3).

For estimation of Kc using satellite data, Kc1 (Trout & Johnson) and Kc2 (Kamble et al.) have relatively larger variation, ranging from around 0.1 to 1, while Kc3 and Kc4 (both from Park et al.) have smaller variation, ranging from approximately 0.2 to 0.6. These calculated satellite Kc values needs to be validated using the in-situ weather station data, which will be the major task for JFY2021.

Table of Contents

List of Figures

Chapter 1: Introduction

This report presents a range of research activities and research outcomes of the project Validation of GCOM-W1 products using global water and energy balance monitoring at the Murray-Darling Basin in Australia during JFY 2020. The project seeks to continue operating the JAXA flux tower within the core validation site located in Yanco, New South Wales, and provide spatially distributed soil moisture data from across an AMSR2 sized footprint. Importantly, this project will also make significant independent and collaborative contributions to i) continuing the validation of the AMSR2 soil moisture product against in-situ observations; ii) Intercomparing the AMSR2 soil moisture product with complimentary satellite soil moisture products from other missions, such as SMAP; and iii) estimating the satellite-based crop coefficient/plant factor Kc using AMSR2 soil moisture product and MODIS vegetation indices.

During JFY2020, the main research activities include flux tower maintenance, data downloading, processing and archive, faulty sensor replacement etc. The processed soil moisture data was used to validate the 10-km and 25-km resolution AMSR2 soil moisture products. On the other hand, we used the NDVI and LAI product from MODIS and the SM product from AMSR2 to estimate the Kc value at the flux tower location (-34.99S 146.29E).

Chapter 2: Flux Tower Maintenance

2.1 Flux Tower Maintenance for JFY 2020

Due to travel restrictions put in place during the COVID-19 pandemic, it was difficult to make site visits to the JAXA Tower during a large part of 2020. Victorian residents were in full lockdown for many months and the state border between New South Wales and Victoria was closed for an extended period.

This meant that monthly visits from Melbourne were impossible. However, in this instance arrangements were made for a local engineer to visit the site and post data cards back to Monash University. As a result, there was fortunately no data loss (gaps) during all of 2020 and early 2021. During times where visits were possible, regular site maintenance was undertaken by a dedicated Monash University Field Technician. This included the following activities:

- cleaning of all environmental sensors within the enclosure
- insect control and cutting grass
- downloading of data, and
- battery health checks.

As a result of Government and University restrictions surrounding travel, field work opportunities were extremely limited for more than one staff member.

Therefore, the calibration of the Gas Analyzer had to be post-poned. As soon as there is an opportunity to have a secondary (trained) technician onsite, the gas analyzer will be removed and calibrated.

2.2 Sensor Condition and Replacement

As outlined in the last annual report, TRIMEPICO32 (at 5cm below ground) was exhibiting some problems. It was replaced on 13th May 2020 with a spare provided by JAXA. It is now functioning well. Other problems that have been encountered in the last fiscal year include the following sensors:

JAXA Tower:

- Campbell Met One 034B Windset (at 8m above ground)
- TRIME-PICO32 soil moisture sensor (at 45cm below ground)

ASSH-T weather station:

- Campbell Met One 034B Windset (at 2m above ground)
- TRIME-PICO32 soil moisture sensore (at 15cm below ground)
- Heat Flux Plate (at 4cm below ground)

All wiring has been checked and there is no obvious physical damage to cabling to explain the faulty sensors. JAXA may decide to provide replacements for the equipment listed.

For most of 2020 conditions of the tower enclosure and surrounding area has been extremely dry with a lot of dry grass growing. The hard ground condition has meant that any digging has been extremely difficult for much of the year. However, the area has just this week received approximately 96.6mm of rain in approximately 3 days causing wet paddock conditions which may last for a few weeks. A visit will be made to site as soon as it is reasonably practical.

Chapter 3: Flux Tower Data

3.1 JAXA Tower Data Archive

Half-hourly measurements from the JAXA flux tower are uploaded from the JAXA station to a Monash server on a weekly basis. Figures below show some of the key data collected in 2020 from the JAXA tower.

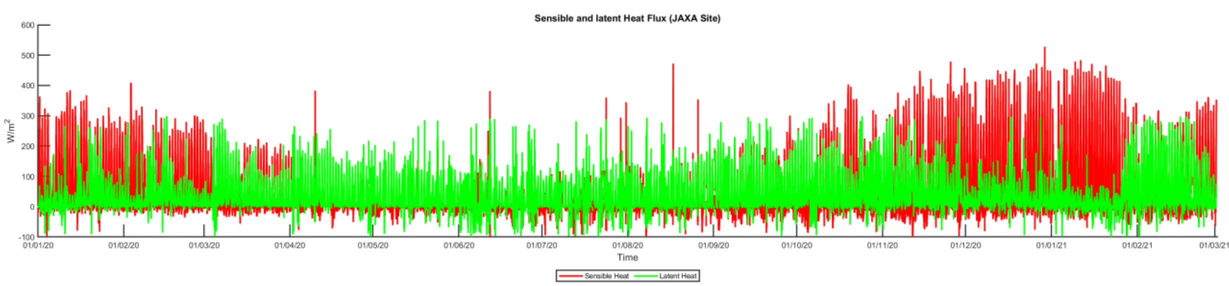

Figure 1: Heat fluxes measured at JAXA Tower for 2020.

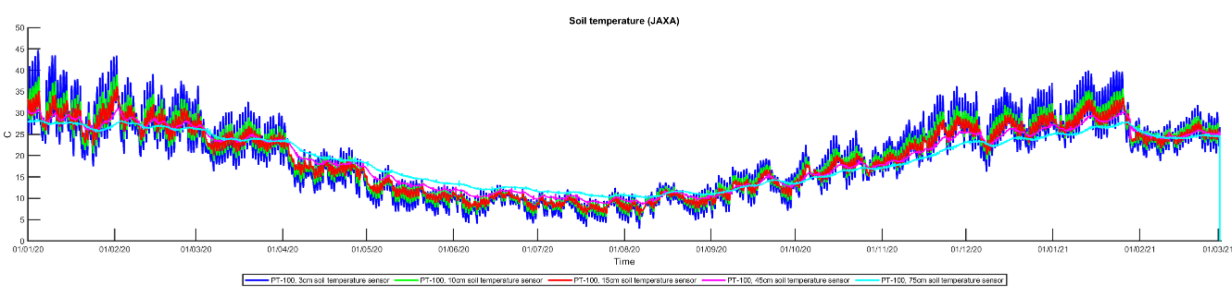

Figure 2: Soil Temperature at JAXA Tower for 2020.

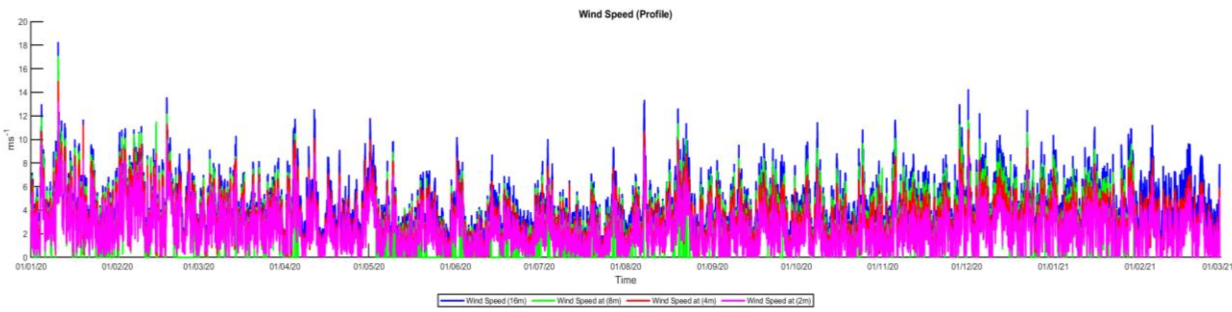

Figure 3: Wind speed at JAXA Tower for 2020.

The TRIME-PICO soil moisture and temperature sensor at 3 cm malfunctioned in May 2020 whereas it was discovered that the erroneous soil moisture measurements from the TRIME-PICO sensor at 45cm has been undetected for quite some time. Measurements of soil temperature form the same sensor however does seems to be within an expected range (Figure 4).

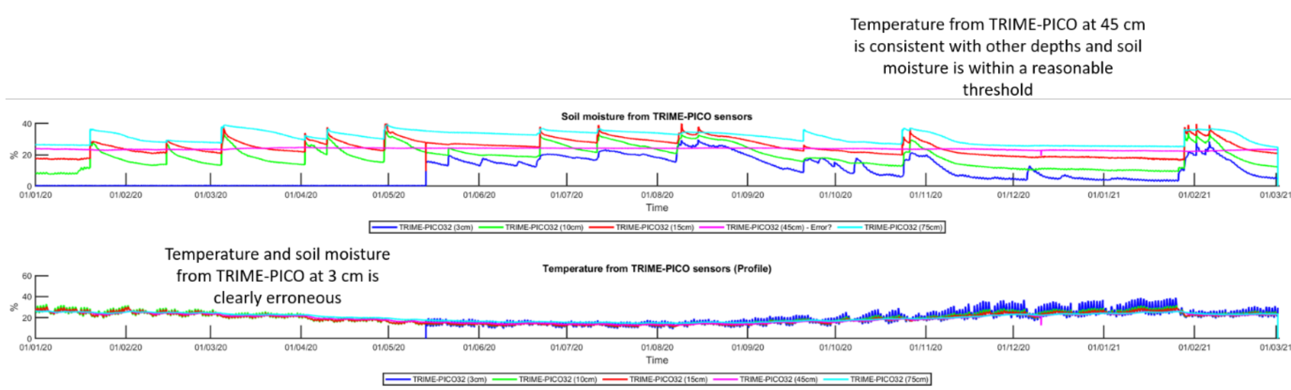

Figure 4: TRIME-PICO soil moisture and temperature measurements at various depths.

The wind vane at 16m at the JAXA tower was stuck between 29th May 2020 to 8th of July 2020 and the issue is now resolved. Wind direction and speed at 8 m was erroneous between the 5th of April to the 3rd of May 2020 and then again on the 29th of January 2021. A site inspection is required to check the cause of this.

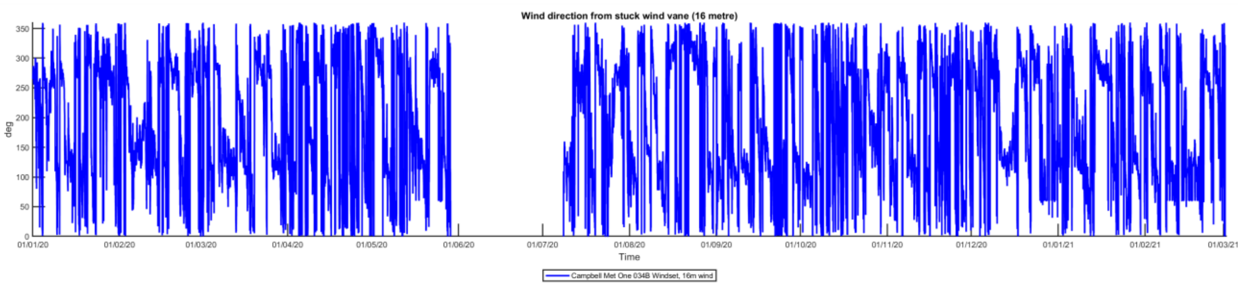

Figure 5: stuck wind vane at 16m height at the JAXA tower station.

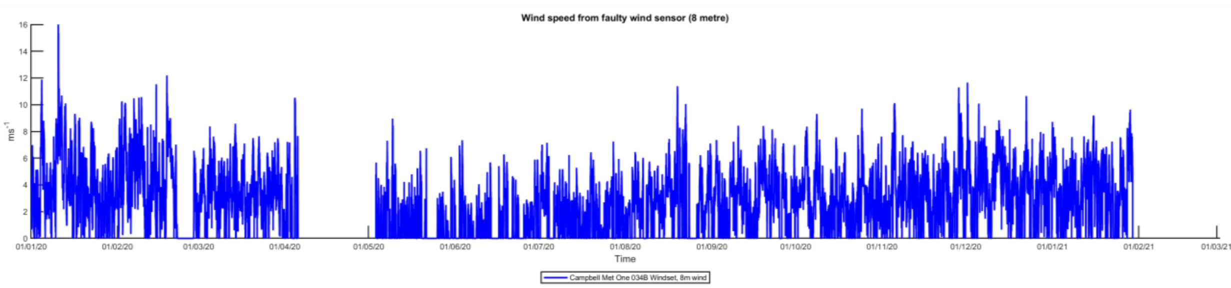

Figure 6: Faulty wind sensor at 8m height at the JAXA tower station.

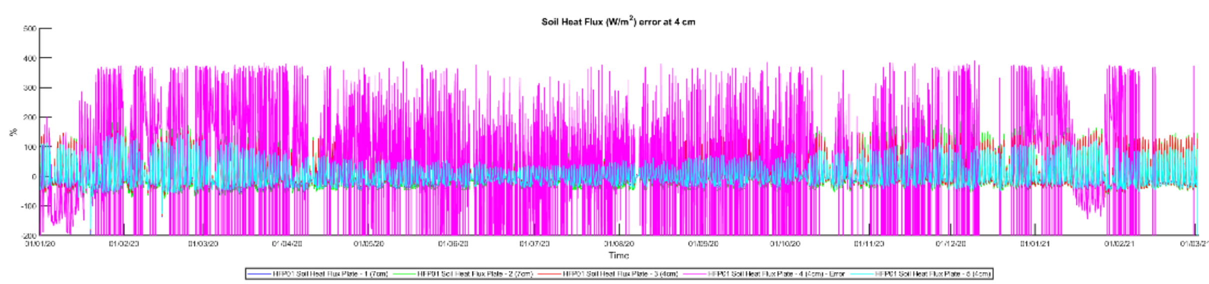

Figure 7: Faulty wind heat flux plate at 4 cm at the JAXA tower station.

The wind sensor at the ASSH-T Weather station malfunctioned from May 2020 (Figure 8). Similarly, TRIME-PICO at 15 cm is not working and needs to be replaced.

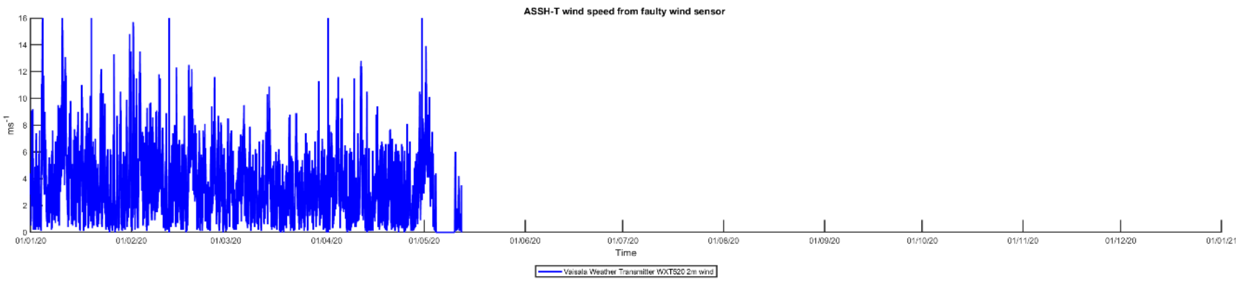

Figure 8: Faulty wind sensor at ASSH-T weather station.

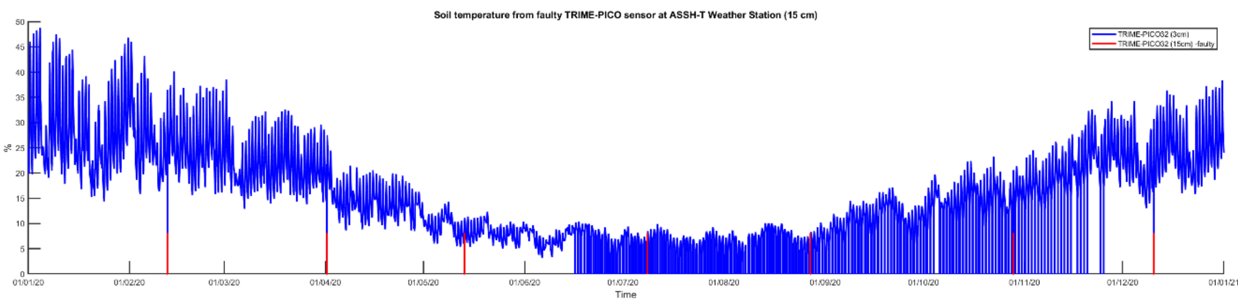

Figure 9: Faulty TRIME-PICO sensor (15 cm) at ASSH-T weather station.

3.2 Real-time Figures Archive

Real-time figures from the flux tower is also produced and available at http://www.science.uwa.edu.au/centres/land/yanco. The website is maintained by Prof. Jason Beringer' s team in Faculty of Science, the University of Western Australia (jason.beringer@uwa.edu.au).

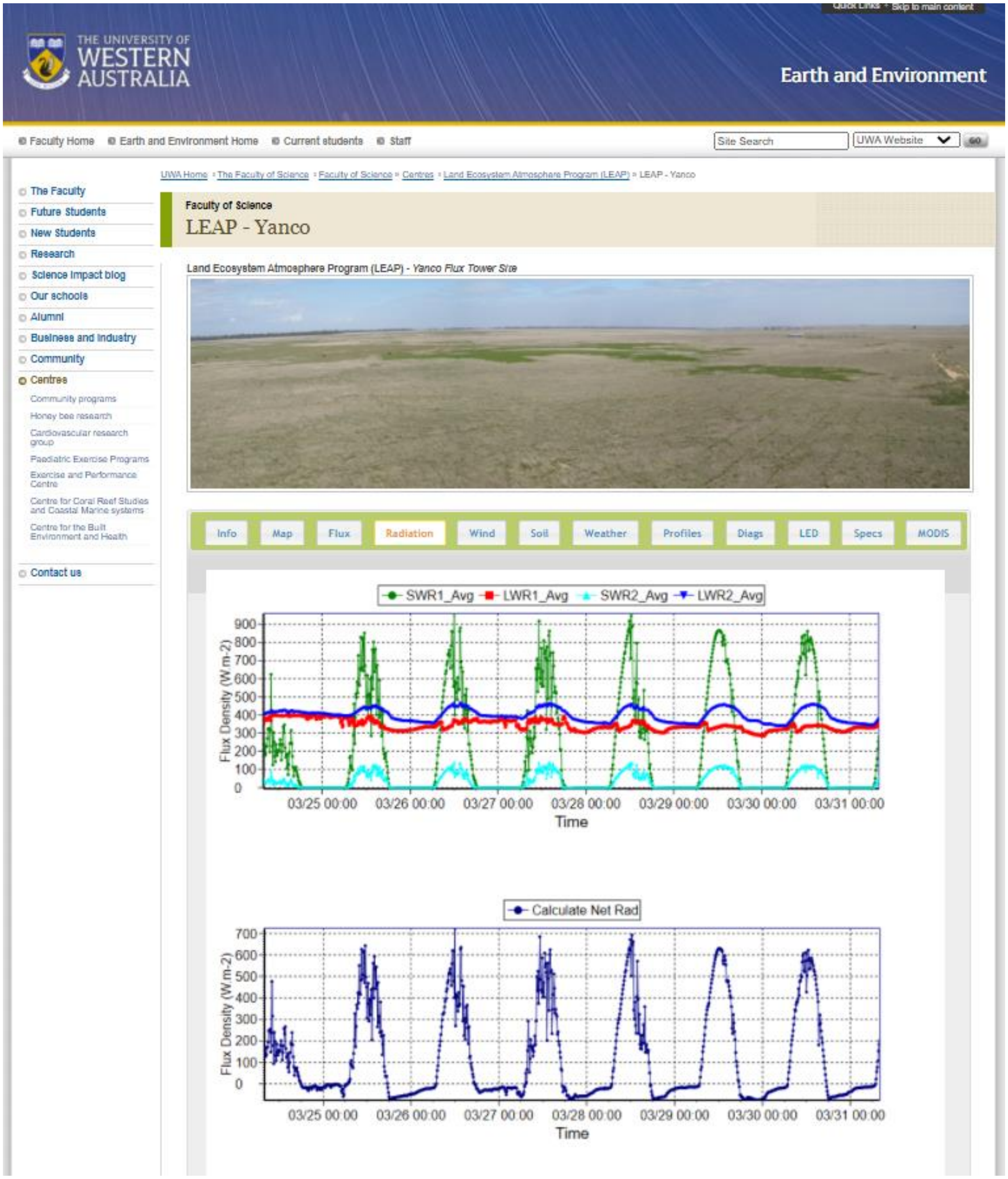

Figure 10: Real-time tower data interface on

http://www.science.uwa.edu.au/centres/land/yanco.

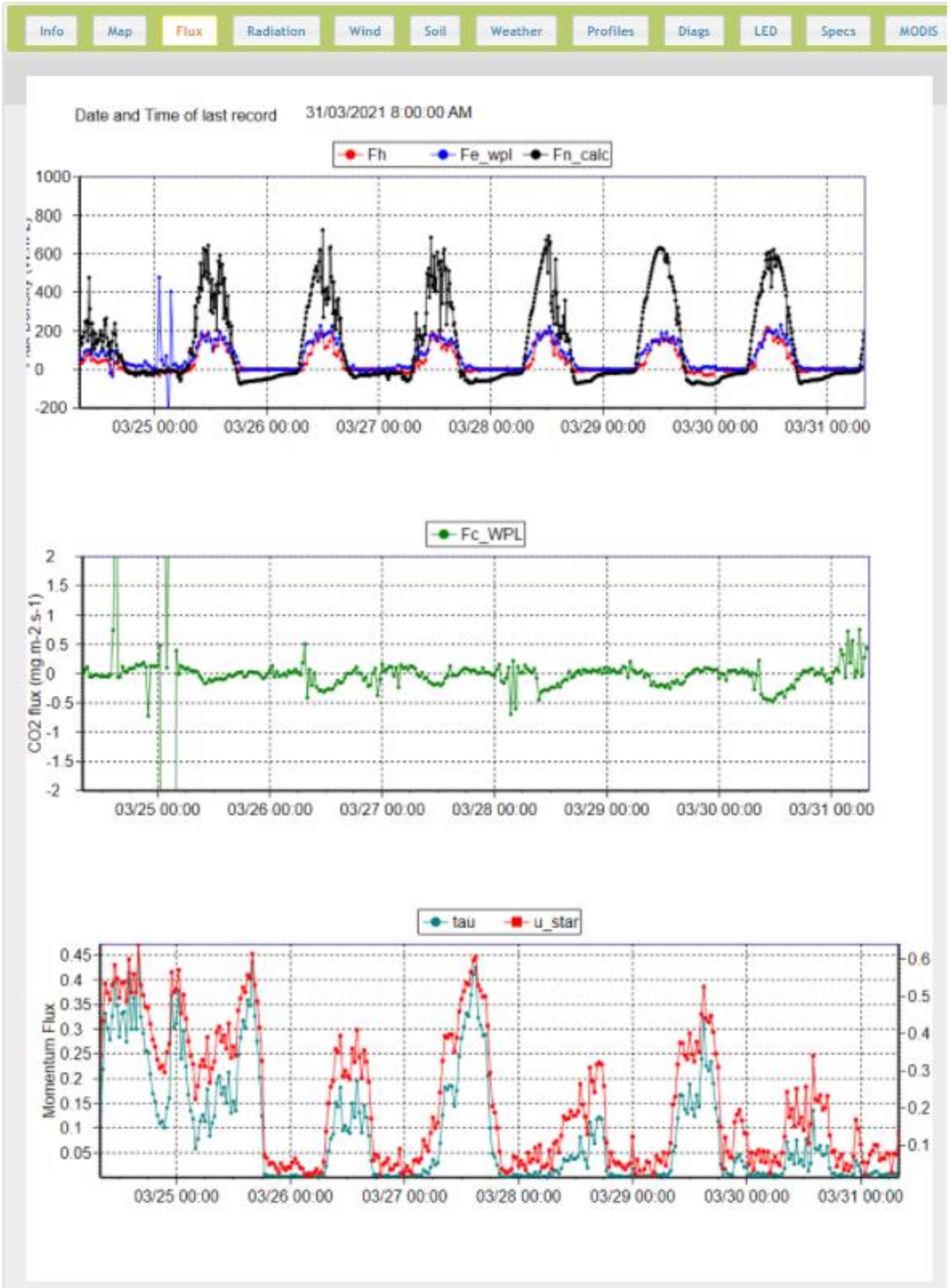

Figure 11: Examples of real-time figures for fluxes.

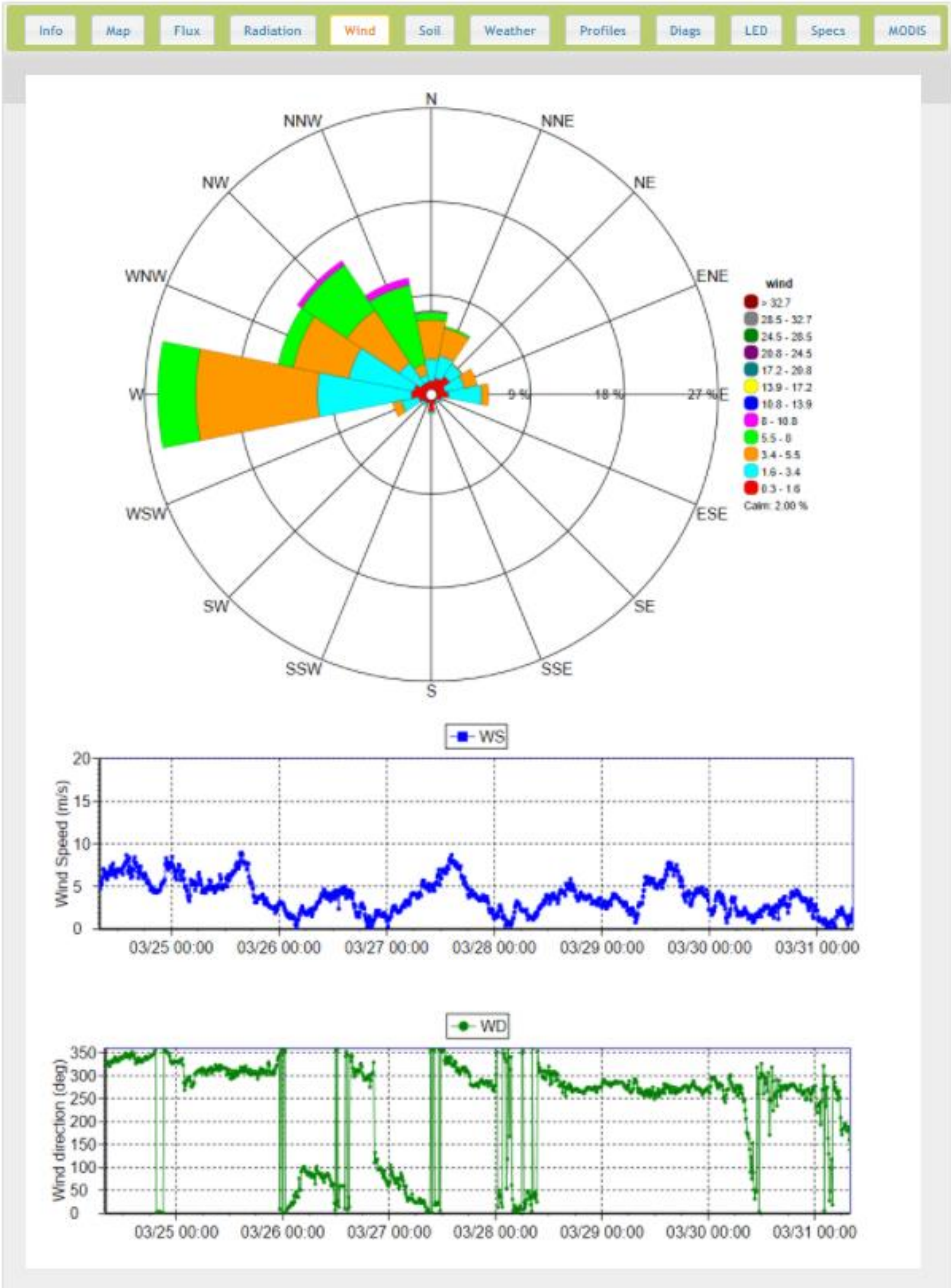

Figure 12: Examples of real-time figures for wind speed and wind direction.

3.3 OzNet monitoring network data

Similar with previous years, soil moisture and soil temperature over 20-min interval of measurements from the OzNet monitoring stations are collected from each station. All raw data have been archived and downloadable at http://www.oznet.org.au.

Data were separated and named according to the southern hemispheric seasons, i.e. spring (September – November), summer (December – February), autumn (March – May) and winter (June – August). Simple quality checks have been applied to these data whereby out of range values have been removed.

Chapter 4: AMSR-2 Level 3 soil moisture products

4.1 The Murrumbidgee Catchment

Located in southern NSW, Australia, the Murrumbidgee catchment is bordered by the Great Dividing Range to the east, the Lachlan catchment to the north, and the Murray catchment to the south. The Murrumbidgee Catchment exhibits a significant spatial variability in climate, soil, vegetation and land cover because of its distinctive topography (Figure 13).

Due to the diversity within this area, the large amount of complementary data from long-term monitoring sites, and past airborne field experiments, this region is an ideal test-bed for the comprehensive validation of satellite soil moisture from missions such as GCOM-W1 and is highly complementary to validation sites in Mongolia and Thailand. Considering the size of the satellite footprint, there are regions in the catchment that are relatively homogeneous in regard to climate, soil type, vegetation, and consequently radiometric response (Rüdiger et al., 2011) when compared to many other countries.

Temporal climatic variations of the catchment are primarily associated with elevation, varying from semi-arid in the west to temperate in the east. The total average annual rainfall for the entire Murrumbidgee River catchment is about 530

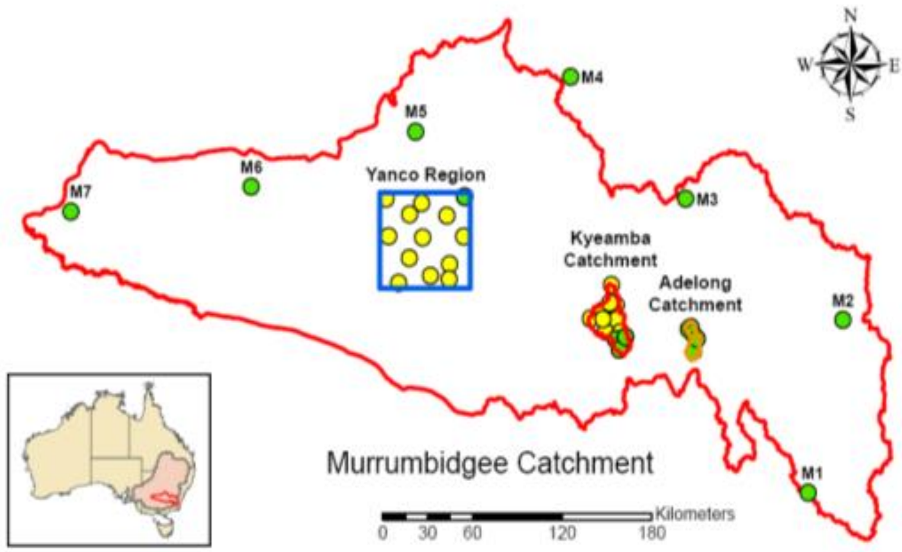

Figure 13: Location of the Yanco core validation site within the Murrumbidgee Catchment. Also shown is the location of the Murrumbidgee Catchment within the Murray-Darling Basin (inset) and the locations of sparse network soil moisture stations.

mm, with a mean annual precipitation of 300 mm in the west and about 1,900 mm towards the east in the Snowy Mountains. The actual evapotranspiration is equivalent to precipitation in the west but represents only half of the precipitation in the east. Long term averaged precipitation data for the Murrumbidgee Catchment shows a relatively constant rate of rainfall across the year, with a slight increase in winter. The Murrumbidgee catchment is characterised by plains in the west with an elevation around 50 m, to steep mountainous regions towards the east with elevations more than 2,100 m in the Snowy Mountains. Soils in the Murrumbidgee Catchment vary from sand to clay, with the western plains being dominated by finer-textured soils and the eastern slopes being dominated by medium-to-coarse textured soils (McKenzie et al., 2000).

Land use in the catchment is predominantly agricultural with the exception of steeper parts, which are dominated by a mixture of native eucalypt forests and exotic forestry plantations. Agricultural land use varies greatly in intensity and includes pastoral, more intensive grazing, broad-acre cropping, and intensive agriculture in irrigation areas along the mid-lower Murrumbidgee. Grazing is predominant in the west and scattered in the east, whereas dryland cropping dominates the mid Murrumbidgee catchment. Irrigation sites are mainly located in western part of the Yanco core validation site. The catchment is comprised of about 52% pasture, followed by about 21% arable and 18% silvicultural land use. The other land use types represent less than 9% of the total catchment area.

4.2 The Yanco Site – location of flux tower

The Yanco area is a 60 km x 60 km area located in the western plains of the Murrumbidgee Catchment where the topography is flat with very few geological outcroppings (Figure 21). Soil types are predominantly clays, red brown earths, transitional red brown earth, sands over clay, and deep sands. Approximately one-third of the core validation site is irrigated during summer when sufficient water is available. The Coleambally Irrigation Area (CIA) is a flat agricultural area of approximately 95,000 hectares that contains more than 500 farms. The principal summer crops grown in the CIA are rice, corn, and soybeans, while winter crops include wheat, barley, oats, and canola. Rice crops are usually flooded in November by about 30 cm of irrigation water.

A total of 24 surface soil moisture sites were installed in late 2009 to develop a nested soil moisture monitoring configuration for the SMAP mission at scales of approximately 3 km, 9 km and 36 km. These stations continuously monitor the soil moisture over the 0-5 cm layer with a Hydraprobe and soil temperature sensors (Unidata® 6507A/10) at 1, 2.5 and 5cm depths. The 24 sites are concentrated on two

9 km x 9 km focus areas (areas YA and YB), corresponding to two pixels of the SMAP grid at which the active passive soil moisture product (SMAP L3_SM_A/P product) was to be produced. Finally, 10 of the sites within areas YA and YB are concentrated on a further two 3 km x 3 km sub-areas (each) with at least 4 stations measuring the distribution of soil moisture across each, corresponding to a total of four of the SMAP radar pixels (see zoomed in figure in Figure 14 for details of the YB area). Unfortunately, the SMAP radar failed shortly after commissioning. However, sentinel data are being used to replace the SMAP radar observations for locations such as the Murray Darling Basin.

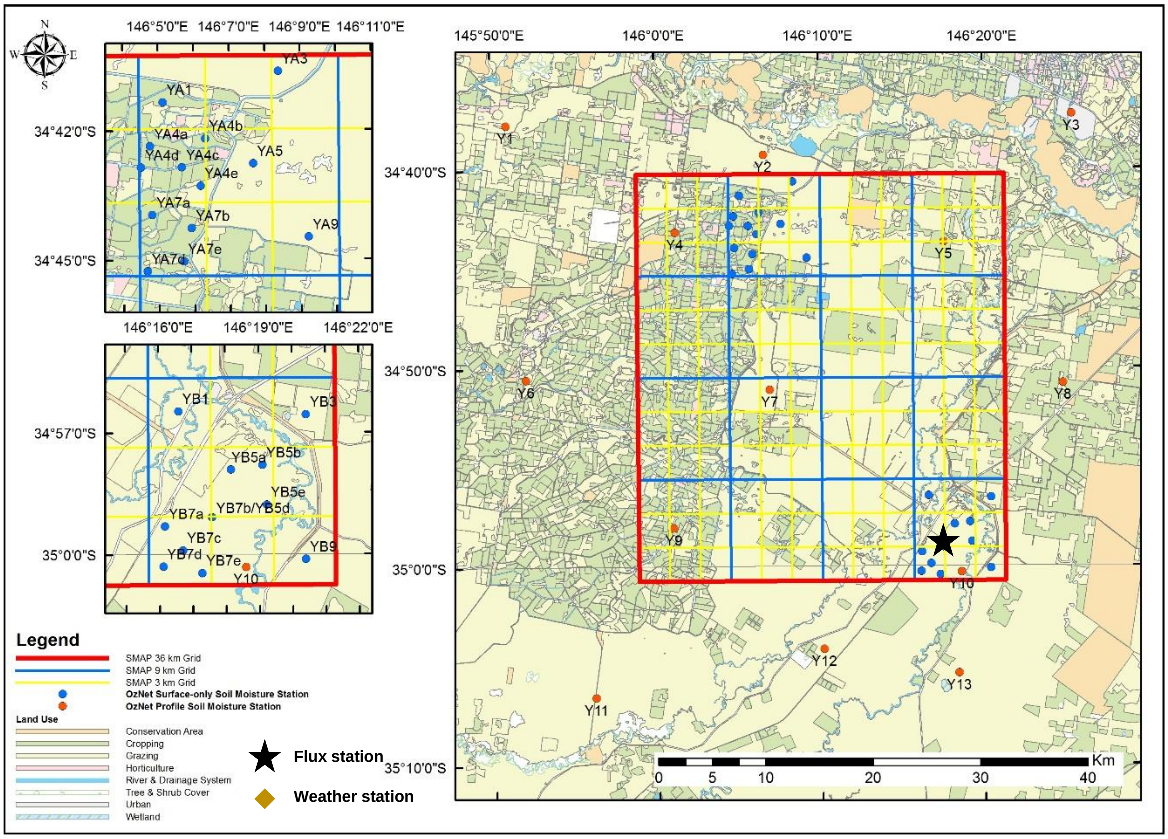

Figure 14: Locations of the JAXA flux station, weather station and soil moisture monitoring stations within the Yanco core validation site. Also shown are the YA and YB focus areas with intensive soil moisture stations, and the locations of intensive ground sampling areas.

This intensive network is also an ideal core validation site for AMSR2, as it i) monitors soil moisture across an AMSR2 sized pixel with approximately 30 stations, and ii) can be used to validate AMSR2 downscaling algorithms through the nested sampling design and supplementary intensive ground sampling activities that have been undertaken. Moreover, extensive airborne data sets and supplementary ground data (see www.smapex. monash.edu) have been used to assess the representativeness of soil moisture sites for each of the 9 km x 9 km focus areas

(areas YA and YB), corresponding to two pixels of the SMAP products at 3 km for radar, 9 km for radar-radiometer and 36 km for radiometer pixels (Yee et al. 2016). These stations have also been used to validate AMSR2 soil moisture products based on the JAXA and LPRM algorithm of different versions, and SMOS soil moisture products (Yee et al., 2016), and provide a perfect source of data for the passive-passive downscaling work proposed here.

4.3 AMSR2 Level 3 soil moisture product

The AMSR2 L3 soil moisture product was downloaded from the GCOM-W1 Data

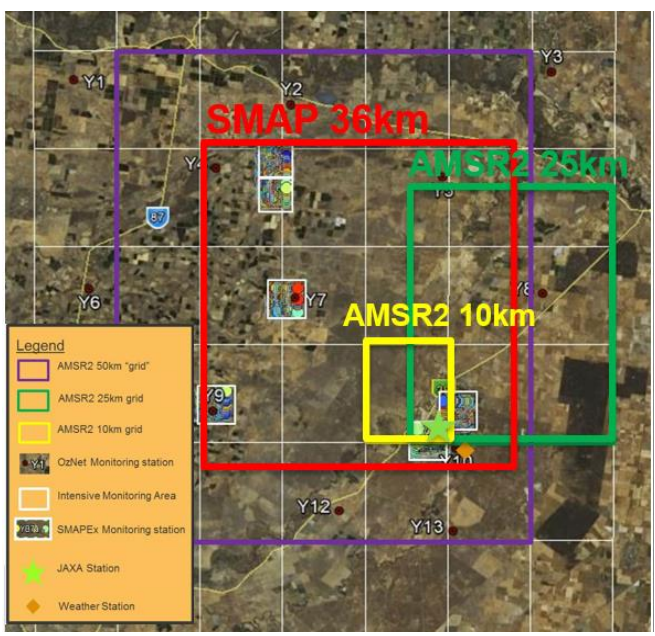

Figure 15: Location of the 10-km and 25-km AMSR2 L3 SMC pixel, SMAP 36-km pixel with respect to the flux tower location.

providing Service (the G-Portal: https://gportal.jaxa.jp/gpr/). To cover the whole period in which AMSR2 data is available, the analysis covered a time series from July 2012 to December 2020 (see Figure 16). Both the high resolution 10-km product and the low resolution 25-km product were considered in the analysis. The product identifier for the 10-km and 25-km resolution data products are 'GW1AM2_YYYYMMDD_01D_EQMD_L3SGSMC**H**F3300300' and 'GW1AM2_ YYYYMMDD_01D_EQMD_L3SGSMC**L**F3300300', respectively.

The AMSR2 pixel in which JAXA tower (-34.99S, 146.29E) is located was extracted. The pixel location of the L3 SM data scene is Row 1250, Column 1463 for the 10-km product, and Row 500, Column 586 for the 25-km product. The pixel boundaries with respect to the flux town location is shown in Figure 15.

The time series of the AMSR2 Level 3 SMC 10-km and 25-km products are shown in Figure 16. It is seen that from 2012 to 2020, 2013-2014 and 2017 are relatedly dry years while the rest of the period are wetter. For the wetter years, comparing with

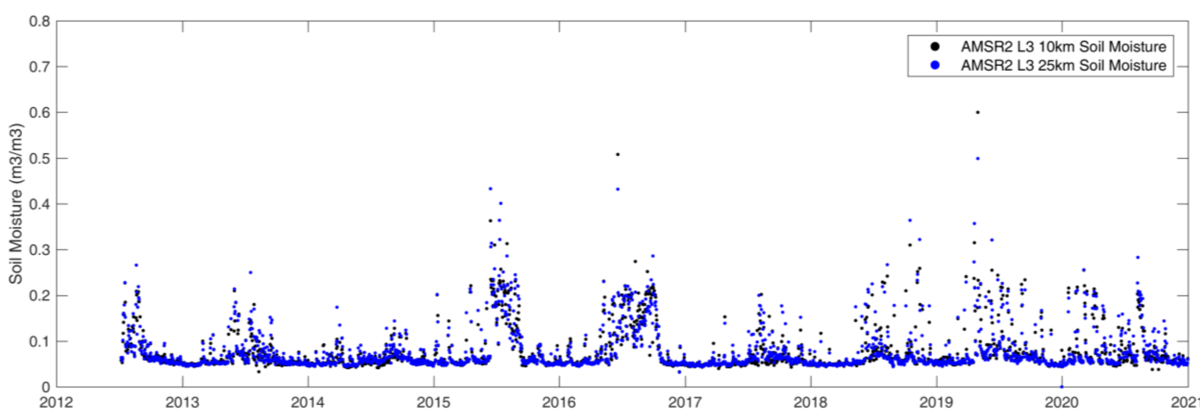

Figure 16: Year 2012 to 2020 time series of the AMSR2 L3 10-km and 25-km soil moisture in the Yanco site.

2015-2016, 2018-2020 experienced a slightly dryer condition throughout the period. But the higher values of 2018-2020 are more scattered. The wet season (May to August) in 2019-2020 is less obvious and has extreme values in rainfall events pretty much throughout the years.

Similar with previous years, the updated 2019-2020 data show that the high-resolution soil moisture almost coincide with the low-resolution data, especially during the dry season. For the wet season, however, the low-resolution soil moisture has a slightly larger dynamic range. This could be due to the reason that 25-km pixel contains a larger area and thus include mixed land cover types such as pasture, crops and forest, while within the 10-km pixel it is almost pasture.

Figure 18 shows the box plots of the AMSR2 L3 low- and high- resolution soil moisture for year 2020 only. Most of data fall in the range of approximately 0.03 m^3/m^3 to 0.12 m^3/m^3 and the median value is only slightly above 0.05 m^3/m^3. Very few data exceed 0.1 m^3/m^3.

Figure 17 shows the box plots of the AMSR2 L3 low- and high- resolution soil moisture for all data from 2012 to 2020. It is seen that most of data fall in the range of approximately 0.04 m^3/m^3 to 0.12 m^3/m^3 and the median value is only slightly above 0.05 m^3/m^3. Very few data exceed 0.2 m^3/m^3 which mostly happened in the winter season of 2015-2016 and 2018-2020, with the highest reaching 0.6 m^3/m^3.

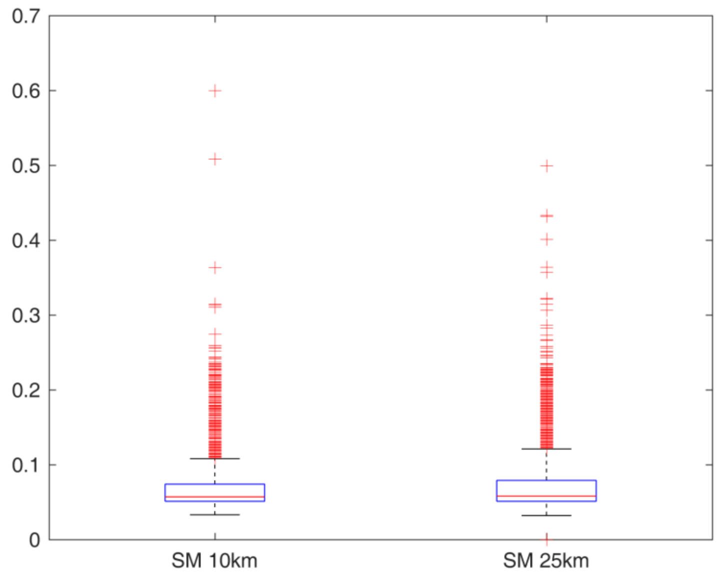

Figure 17: Box plot of the AMSR2 L3 10-km and 25-km soil moisture in the Yanco site: 2012-2020.

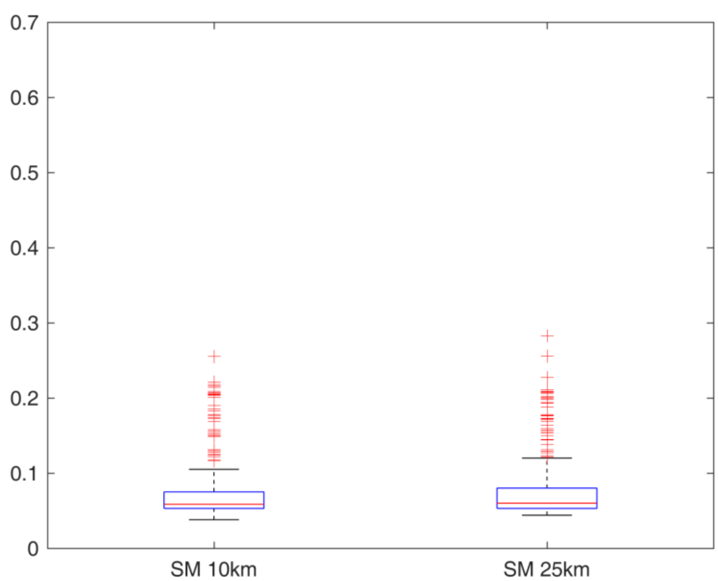

Figure 18: Box plot of the AMSR2 L3 10-km and 25-km soil moisture in the Yanco site: year 2020 only.

Chapter 5: Validation of AMSR-2 Level 3 Soil Moisture Products

5.1 Time Series Plots

The AMSR2 L3 10km- and 25km- soil moisture products are validated against 1) the in-situ soil moisture measurements from the JAXA flux tower, and 2) SMAP observations.

Figure 19 shows a time series plot of the comparison of AMSR2 SM against flux tower SM from July 2012 to December 2020 (flux tower SM data missing for the first couple of months in 2020 due to broken TRIME-PICO sensor). On the flux tower, soil moisture sensor was installed at 3 cm depth below ground. It can be seen that the AMSR2 products are underestimating the tower soil moisture (red) in general. The correlation is relatively higher during the dry period of all years. Compared to tower SM, similar with previous years, in 2019-2020, lower values match better than the higher values. For 2019-2020, there was clear gap between tower and AMSR2 in wet season, similar to 2015-2016. There is also a clear trend of increasing and decreasing in tower SM throughout the wet season, while trend is not clear in the AMSR2 product.

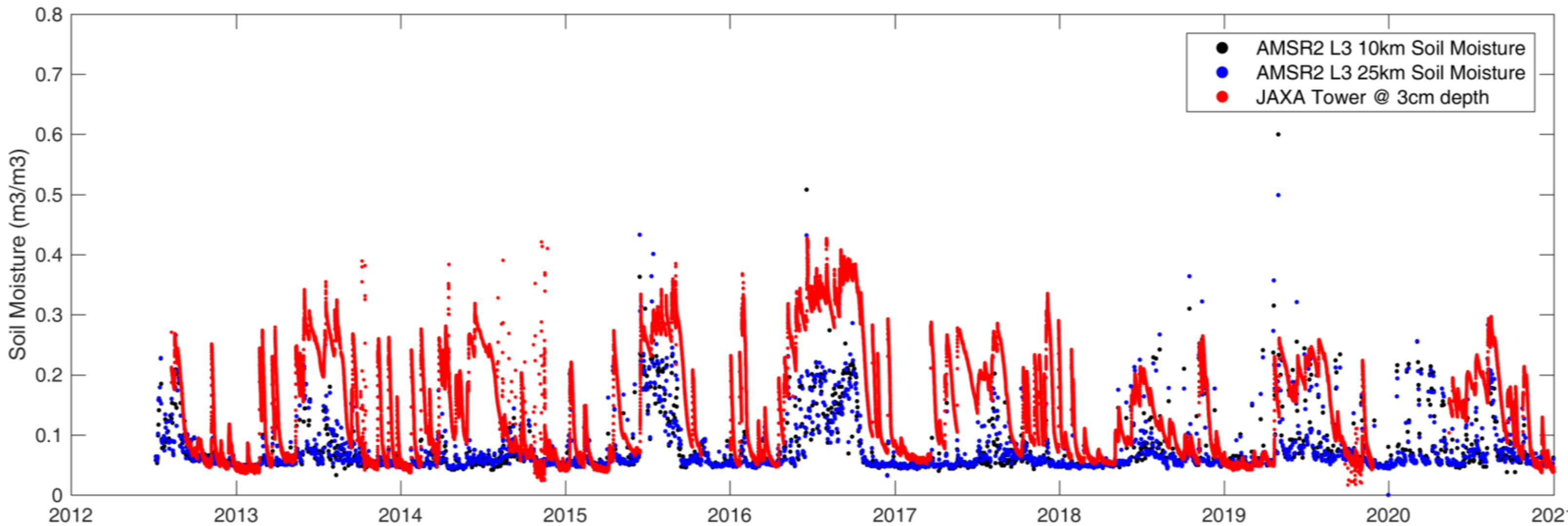

Figure 19: Time series plot of AMSR2 L3 10- and 25-km soil moisture product against JAXA flux tower soil moisture measured at 3-cm depth from 2012 to 2020.

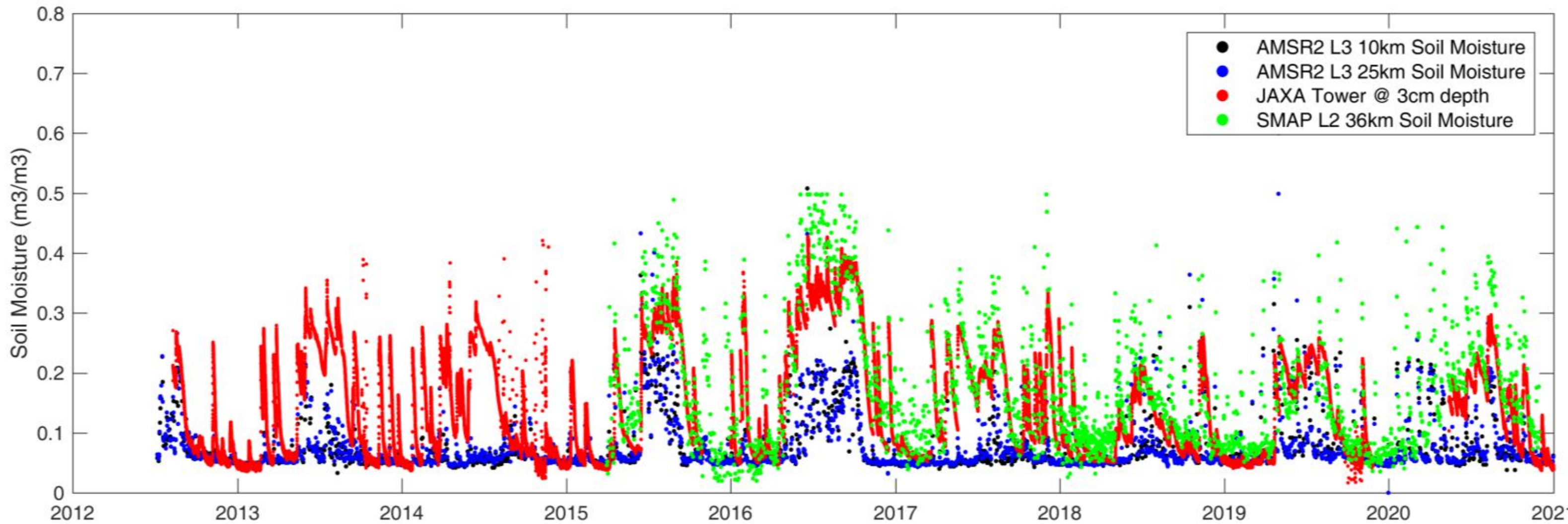

Figure 20: Same time series plot as Figure 19 with added SMAP L2 36km soil moisture product from 2012 to 2020.

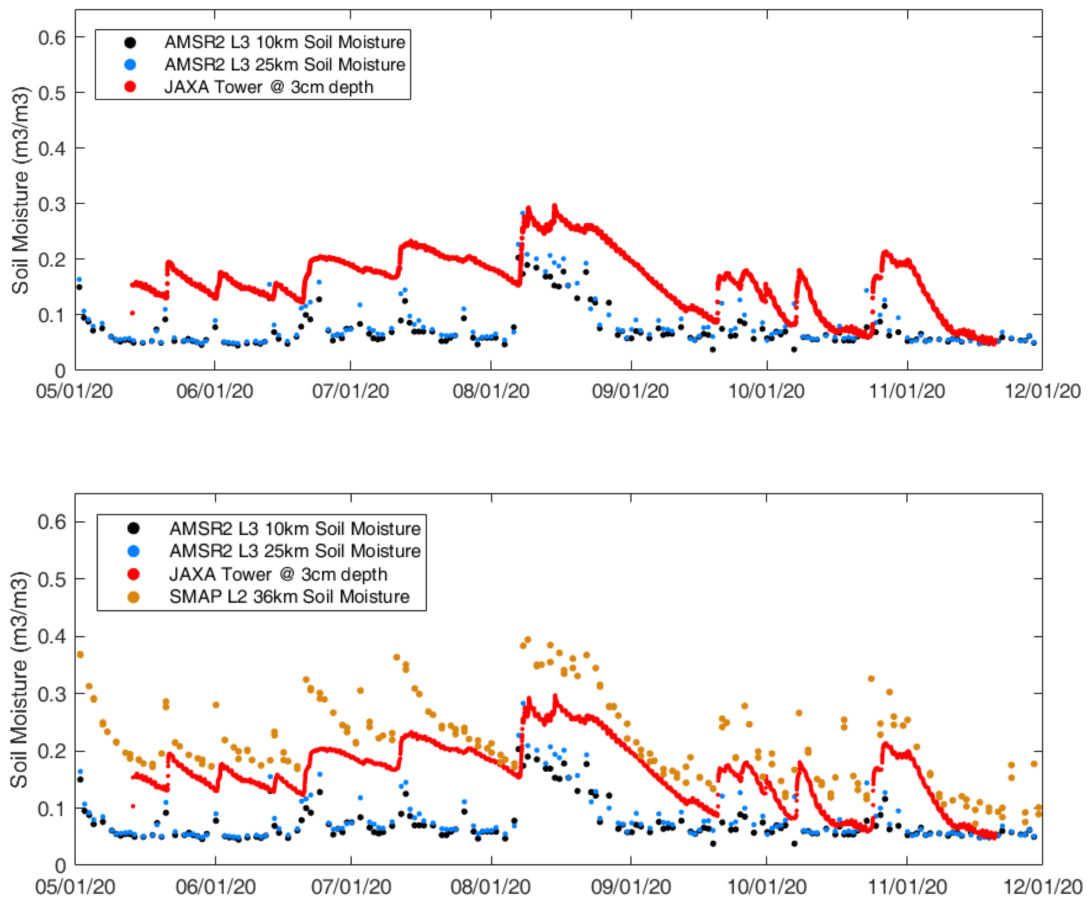

Figure 21: Zoom-in view of time series of AMSR2 products, tower SM and SMAP SM for 2020 only (Jan-Apr deleted as tower SM data missing due to broken sensor).

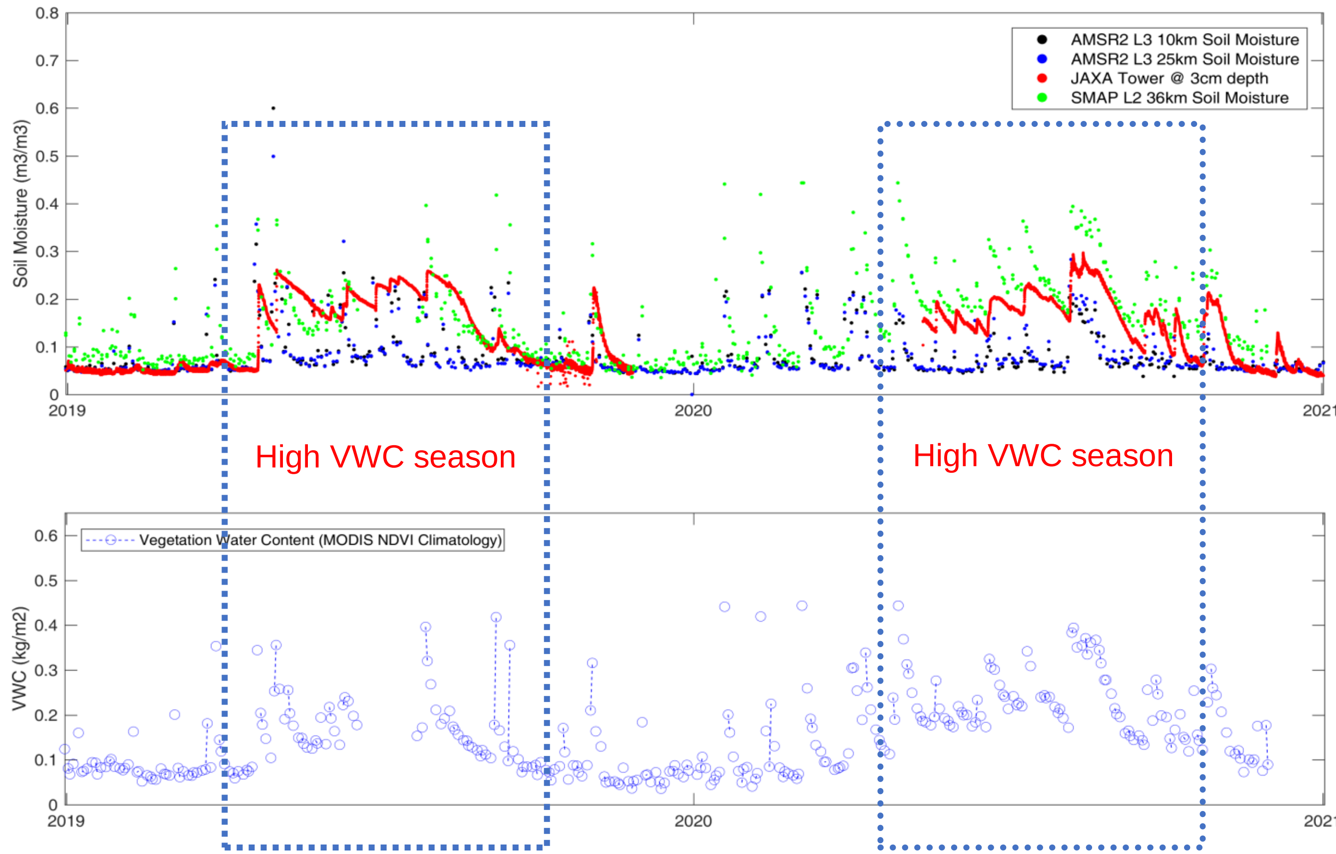

Figure 22: Soil moisture time series plot during 2019-2020 in comparison with VWC for the same period.

Figure 20 added the Soil Moisture Active Passive (SMAP) L2 36km (passive-only algorithm) product to Figure 19. The product was retrieved from L-band (1.4 GHz) brightness temperature observations.

Having a larger footprint of 36 km compared with the AMSR2 products, it can be seen that the SMAP product (green) matches better with tower soil moisture compared to AMSR2 itself, especially for wet seasons (May-Sept). For dry season, however, SMAP overestimates the soil moisture 'truth' while AMSR2 matches slightly better. Since the AMSR2 soil moisture was retrieved from C-band, which is a higher frequency, the signal is more affected by the vegetation layer and thus it is more difficult to decouple the effect of vegetation (more pronounced during wet season) from soil moisture.

As it has also been widely demonstrated in the past that low frequency (L-band) has higher sensitivity to the moisture content variation and more capable to retrieve accurate surface soil moisture, it is suggested that the SMAP product should be closer to the ground 'truth',

For the year 2020 in particular, Figure 21 shows a time series plot of AMSR2 SM compared against flux tower SM at 3cm depth from May 2020 to December 2020. It can be seen that in general the AMSR2 products (black for 10 km and blue for 25 km) are underestimating the tower soil moisture (red). The correlation is relatively better during the dry period (Oct-Dec) compared with the wet season (May-Sept).

As also mentioned in the annual report of JFY 2018 and 2019, one possible way for improving the AMSR2 soil moisture product is through applying a simple regression of itself against in-situ measurement based on the historical data profile. This regression could be set to apply to the original product once soil moisture exceeds certain level, e.g. 0.1 m^3/m^3, beyond which the product/in-situ discrepancy starts to become more pronounced.

Figure 22 shows the soil moisture time series plot during 2019-2020 in comparison with VWC for the same period. Looking at the two years' data only, it is more obvious that the accuracy is lower during wet seasons. The VWC derived from MODIS 10-year NDVI climatology is also plotted to compared with the soil moisture trend. Here the VWC trend matches well with the soil moisture trend; the peaks of VWC also correlate well with the soil moisture peaks. Since the AMSR2 soil moisture was retrieved from C-band, which is a higher frequency, the signal is more affected by the vegetation layer and thus it is more difficult to decouple the effect of vegetation from SM. Therefore, it is less sensitive to the soil moisture change.

5.2 Scatter Plots and Statistics

The AMSR2 L3 soil moisture product at 10-km resolution are also plotted in Figure 23 as scatters against soil moisture observations from tower (Fig 23a) and SMAP (Fig 23b). It shows negative bias similar to in the time series plot. Tower soil moisture is also plotted against SMAP SM (Fig 23c). When comparing SMAP SM to tower SM, the bias was smaller and both RMSE and correlation were relatively higher.

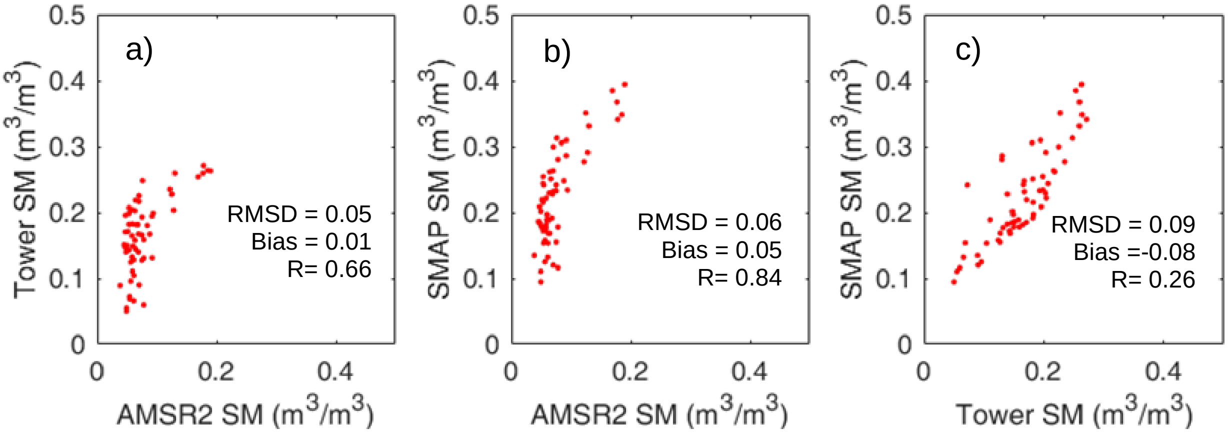

Figure 23: Scatter plots of AMSR2 SM (10-km) against a) tower soil moisture, b) SMAP SM (36km), and c) tower SM against SMAP SM.

Chapter 6: Development of Satellite Kc using AMSR2 SMC product

6.1 The Importance of Kc

Crop water requirements (ETc) can be estimated considering a climatic parameter called reference evapotranspiration (ETo), which represents the evapotranspiration from a standardize vegetated surface, and a crop factor called crop coefficient (Kc) that relates ETc to ETo by the equation (Allen et al., 1998):

$$ETc = ETo \times Kc$$

ETo is the rate that an extensive surface of green, well-watered grass of uniform height, actively growing and completely shading the ground evaporates water. As soil factors do not affect this reference surface, the only factors affecting ETo are climatic parameters (radiation, air temperature, humidity and wind speed above all) which can be obtained from weather station data.

Different ETc can result between crops even under the same environmental conditions due to differences in height, canopy architecture, ground cover, and development stage. Kc incorporates the non-weather factors such as canopy architecture, crop-soil resistance and row spacings that cause ETc vary from ETo into the equation.

Determining Kc by direct methods (lysimeters, energy balance, and soil water balance) for a specific crop in a single location is expensive and not easy to do. Therefore generic Kc values are typically used, which often do not match the actual crop/plant water use. This is due to the reasons such as differences in canopy management, row spacings, and agronomic management. Indirect methods, however, can be used for this purpose to provide site specific crop coefficients.

Kc has been shown to be closely related to the canopy ground cover fraction (i.e. light interception) which can be estimated from remote sensing measurements of the Normalized Difference Vegetation Index (NDVI).

Thus, this chapter integrates information from satellite sources and estimate Kc.

6.2 The Estimation of Kc

The spectral distribution of the light reflected from plant canopies contains information that can be useful for monitoring canopy growth, transpiration, photosynthesis and for diagnosis of biotic and abiotic stresses. Leaf structure and its components such as chlorophyll or other pigments (carotenoids, anthocyanins, etc.) have an effect on the absorption of light. Leaves absorb most of the visible electromagnetic energy (less in the green region which is the reason why vegetation appears green to ours eyes) but reflects a large part of the energy in the near-infrared spectrum, which makes its spectral reflectance different from that of soil or water. Green vegetation shows relatively low reflectance in visible wavelength and a suddenly increase at around red-edge (700 nm) while soil tends to show a steadily increasing reflectance with increasing wavelength (Jones 2014).

Fully developed vegetation canopies tend to have less reflectance in the red spectrum (R) and higher reflectance in the near-infrared spectrum (NIR) as compared to developing canopies. This relationship is the base of the vegetation index known as NDVI, which is the mathematical combination of the R and NIR spectral bands as follows (Rouse et al., 1974):

$$NDVI = (NIR-R) / (NIR+R)$$

NDVI has been strongly correlated with crop canopy cover for various crops in semi-arid areas and can be converted to Kc values by a number of different empirical relationships as below:

1) $Kc = 1.37\ NDVI – 0.086$ (Trout & Johnson, 2007)

2) $Kc = 1.457\ NDVI – 0.1725$ (Kamble et al, 2013)

3) $Kc = 1.621\ SM + 0.471\ NDVI + 0.017\ LAI$ (Park et al, 2017)

4) $Kc = 1.552\ SM + 0.211\ NDVI + 0.009\ LAI$ (Park et al, 2017)

In this study, we will use the NDVI and LAI product from MODIS and the SM product from AMSR2 to estimate the Kc value at tower location (-34.99S 146.29E). The AMSR2 product used is the 10km L3 SMC product. The NDVI product is the MODIS 16-day 1km resolution product (MOD13A2) and the LAI product is the 8-day LAI 1km resolution product (MOD15A2).

6.3 The Estimated Kc Result

In this study, we will use the NDVI and LAI product from MODIS and the SM product from AMSR2 to estimate the Kc value at tower location (-34.99S 146.29E). The AMSR2 product used is the 10km L3 SMC product. The NDVI product is the MODIS 16-day 1km resolution product (MOD13A2) and the LAI product is the 8-day LAI 1km resolution product (MOD15A2).

The satellite data including SM, NDVI and LAI are plotted in Figure 24 for the period 2012-2020. It is seen that LAI and NDVI are highly correlated and have similar dynamic range, with values peaking around July-September each year and valleying around December-January. It is also clear that year 2018 had experienced a very low vegetation level throughout the year, while the winter of 2020 had seen the highest level of vegetation. The variation of AMSR2 SM is less dynamic but still follows similar trend compared to NDVI and LAI.

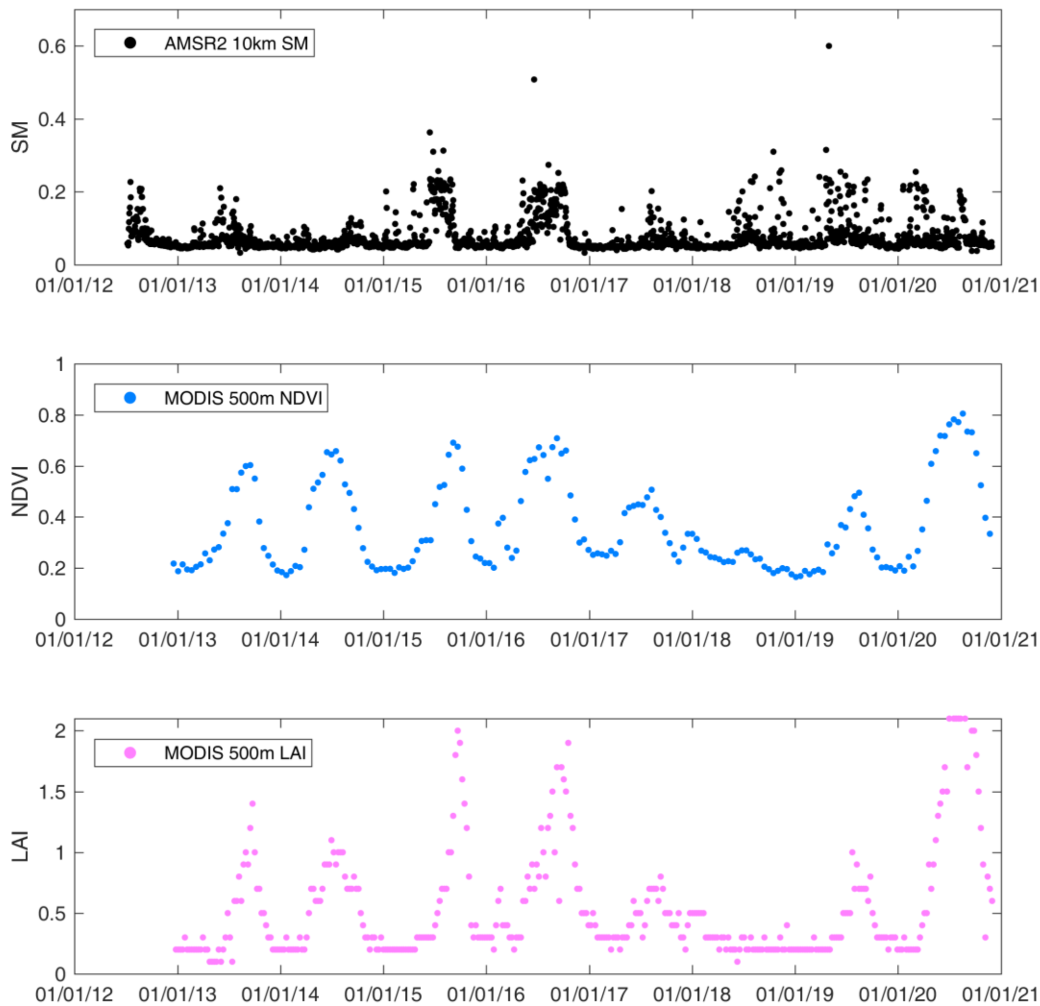

Figure 24: Satellite data input for Kc estimation: 1) SM from AMSR2, 2) NDVI from MODIS and 3) LAI from MODIS from 2012 to 2020

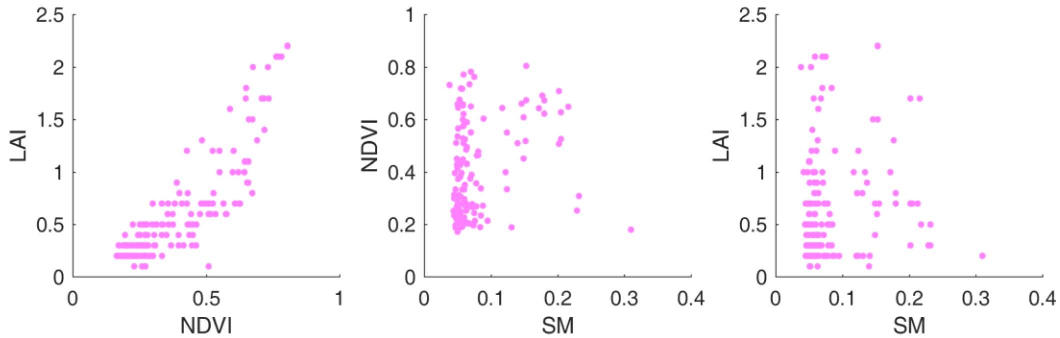

Figure 25: Scatter plot of (1) NDVI against LAI; (2) SM against NDVI, and (3) SM against LAI.

Scatter plots of the same sate sets are shown in Figure 25. It also shows that LAI and NDVI are highly correlated, while SM is not quite correlated with NDVI or LAI.

The calculated Kc using the four different methods are shown in Figure 26. It is clear that Kc1, Kc2, Kc3 and Kc4 all follow the same trend but with different dynamic range. Kc1 and Kc2 have relatively larger variation, ranging from around 0.1 to 1, while Kc3 and Kc4 have smaller variation, ranging from approximately 0.2 to 0.6.

These calculated satellite Kc values needs to be validated using the in-situ weather station data, which will be the major task for JFY2021. The comparison of satellite Kc and in-situ Kc will be included in next year's annual report.

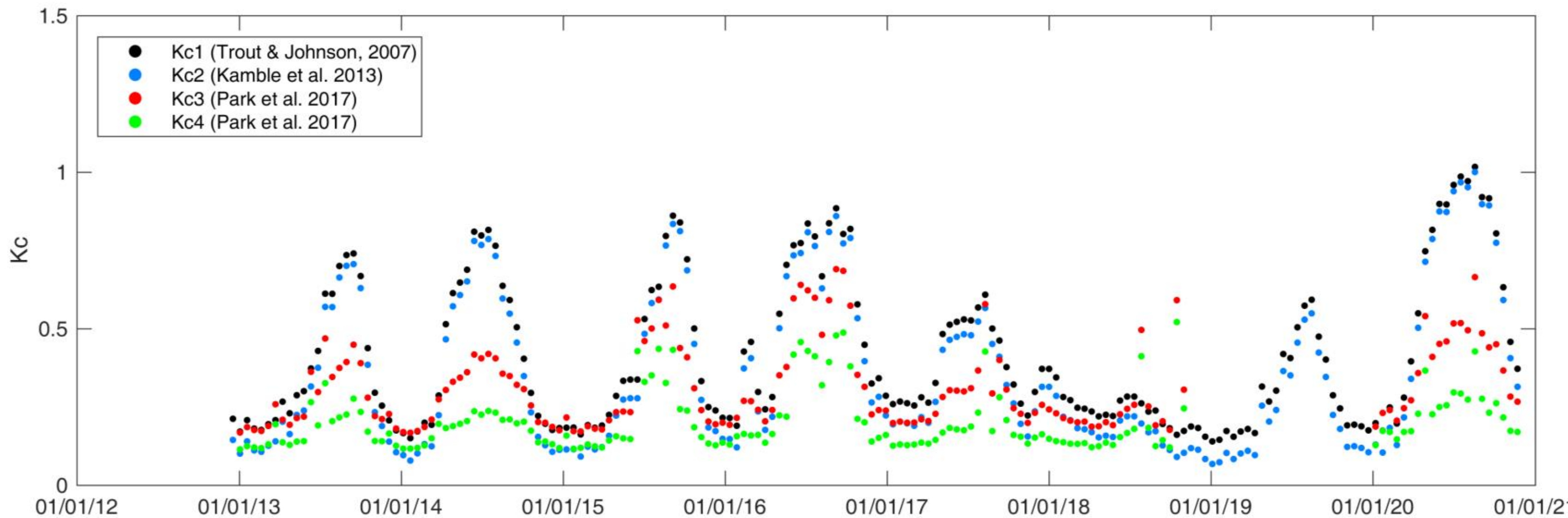

Figure 26: Calculated Kc over the period 2012-2020 using four different methods from literature.

Chapter 7: Future Work

Apart from validation of the AMSR2 soil moisture, there will be two major tasks in JFY2021: 1) estimation of the in-situ Kc and compare with the satellite Kc, and 2) validation of the AMSR2 VWC product.

1. Calculation of in-situ Kc

- Kc = ETc / ETo. ETc is crop evapotranspiration, which can be obtained from the flux tower EC; ETo is reference evapotranspiration, which can be calculated from FAO Penman-Monteith equation, with flux tower data such as wind speed, air T, soil heat fluxes etc.

$$ET_0 = \frac{0.408\Delta(R_n - G)\gamma \frac{C_n}{T_a + 273} U_2(e_s - e_a)}{\Delta + \gamma(1 + C_d U_2)}$$

eq (10)

Rn: net radiation at the crop surface

G: soil heat flux density (MJ m^2/day)

T: air temperature at 2m height (°C)

U_2: wind speed at 2m height (m/s)

e_s: saturation vapor pressure (kPa)

e_a: actual vapor pressure (kPa)

e_s- e_a: saturation vapor deficit (kPa)

Δ: slope vapor pressure curve (kPa/ ^{o}C)

γ: psychometric constant

C_n: numerator constant

C_d: denominator constant

2. Validation of AMSR2 VWC product

According JAXA this product just became available so this work can be completed in JFY2021. The target is to validate the AMSR2 VWC research product at 10km resolution.

The proposed methodology includes two main aspects: validation of AMSR-2 VWC with calculated VWC from MODIS vegetation indices (e.g. from NDVI and NDWIs using equations from Gao et al, 2015); and validation of AMSR-2 VWC with field sampling collected from SMAPEx-4 and SMAPEx-5 field campaigns at Yanco area.

Chapter 8: Summary and Conclusion

This report presents the JFY 2020 research results for the project 'Validation of global water and energy balance monitoring in the Australian Murray-Darling Basin using GCOM-W1 data'. During JFY 2020, this project focused on: i) Continuing the validation of the AMSR2 soil moisture product against in-situ observations, ii) Intercomparing the AMSR2 soil moisture product with complimentary satellite soil moisture products from other missions, such as SMAP, and iii) estimating satellite Kc using AMSR2 SM product and MODIS vegetation indices.

Results indicated that the AMSR2 L3 soil moisture product match with the JAXA tower and in-situ station measurements relatively well during the dry season which is very similar with previous years (when soil moisture is smaller than 0.1 m^3/m^3). For 2019-2020, AMSR2 L3 product (10km & 25km) still underestimates the soil moisture when compared with the tower measurements and representative stations, especially during wet season (soil moisture ranges from 0.1-0.4 m^3/m^3).

For estimation of Kc using satellite data, Kc1, Kc2, Kc3 and Kc4 all follow the same trend but with different dynamic range. Kc1 (Trout & Johnson) and Kc2

(Kamble et al.) have relatively larger variation, ranging from around 0.1 to 1, while Kc3 and Kc4 (both from Park et al.) have smaller variation, ranging from approximately 0.2 to 0.6. These calculated satellite Kc values needs to be validated using the in-situ weather station data, which will be the major task for JFY2021.

List of Publications

Below is a list of recent publications that are related to this research and the JAXA flux station/Oznet/Ozflux network:

1. Cleverly, J., Vote, C., Isaac, P., Ewenz, C., Harahap, M., Beringer, J., Campbell, D. I., Daly, E., Eamus, E., He, L., Hunt, J., Grace, P., Hutley, L. B., Laubach, J., McCaskill, M., Rowlings, D., Jonker, S. R., Schipper, L. A., Schroder, I., Teodosio, B., Yu, Q., Ward, P. R., Walker, J. P., Webb, J. A., Grover, S. P. P., 2020. Carbon, Water and Energy Fluxes in Agricultural Systems of Australia and New Zealand, Agriculture and Forest Meteorology, 287: 107934

2. Pastorello, G. et al., 2020. The FLUXNET2015 Dataset and the ONEFlux Processing Pipeline for Eddy Covariance Data, Nature – Scientific Data, 7(225): 27pp. (pdf 2.7MB)

3. Griebel A, Metzen D, Pendall E, Burba G, Metzger S. 2020. Generating Spatially Robust Carbon Budgets From Flux Tower Observations. Geophysical Research Letters 47:e2019GL085942. DOI: 10.1029/2019GL085942.

4. Li X, Xiao JF, He BB, Arain MA, Beringer J, Desai AR, Emmel C, Hollinger DY, Krasnova A, Mammarella I, Noe SM, Ortiz PS, Rey-Sanchez AC, Rocha AV, Varlagin A. 2018. Solar-induced chlorophyll fluorescence is strongly correlated with terrestrial photosynthesis for a wide variety of biomes: First global analysis based on OCO-2 and flux tower observations. Global Change Biology 24:3990-4008. DOI: 10.1111/gcb.14297.

5. Lin H, Tu C, Fang J, Gioli B, Loubet B, Gruening C, Zhou G, Beringer J, Huang J, Dušek J, Liddell M, Buysse P, Shi P, Song Q, Han S, Magliulo V, Li Y, Grace J. 2020. Forests buffer thermal fluctuation better than non-forests. Agricultural and Forest Meteorology 288-289:107994. DOI: 10.1016/j.agrformet.2020.107994.

6. Lin S, Li J, Liu Q, Li L, Zhao J, Yu W. 2019. Evaluating the Effectiveness of Using Vegetation Indices Based on Red-Edge Reflectance from Sentinel-2 to Estimate Gross Primary Productivity. Remote Sensing 11. DOI: 10.3390/rs11111303.

7. Maes WH, Gentine P, Verhoest NEC, Miralles DG. 2019. Potential evaporation at eddy-covariance sites across the globe. Hydrology and Earth System Sciences 23:925-948. DOI: 10.5194/hess-23-925-2019.

8. McColl KA, Rigden AJ. 2020. Emergent Simplicity of Continental Evapotranspiration. Geophysical Research Letters 47:e2020GL087101. DOI: 10.1029/2020GL087101.

9. van der Horst SVJ, Pitman AJ, De Kauwe MG, Ukkola A, Abramowitz G, Isaac P. 2019. How representative are FLUXNET measurements of surface fluxes during temperature extremes? Biogeosciences 16:1829-1844. DOI: 10.5194/bg-16-1829-2019.

10. Xiao M, Yu Z, Kong D, Gu X, Mammarella I, Montagnani L, Arain MA, Merbold L, Magliulo V, Lohila A, Buchmann N, Wolf S, Gharun M, Hörtnagl L, Beringer J, Gioli B. 2020. Stomatal response to decreased relative humidity constrains the acceleration of terrestrial evapotranspiration. Environmental Research Letters 15:094066. DOI: 10.1088/1748-9326/ab9967.

11. Pastorello G, Trotta C, Canfora E, Chu H, Christianson D, Cheah Y-W, Poindexter C, Chen J, Elbashandy A, Humphrey M, Isaac P, Polidori D, Ribeca A, van Ingen C, Zhang L, Amiro B, Ammann C, Arain MA, Ardö J, Arkebauer T, Arndt SK, Arriga N, Aubinet M, Aurela M, Baldocchi D, Barr A, Beamesderfer E, Marchesini LB, Bergeron O, Beringer J, Bernhofer C, Berveiller D, Billesbach D, Black TA, Blanken PD, Bohrer G, Boike J, Bolstad PV, Bonal D, Bonnefond J-M, Bowling DR, Bracho R, Brodeur J, Brümmer C, Buchmann N, Burban B, Burns SP, Buysse P, Cale P, Cavagna M, Cellier P, Chen S, Chini I, Christensen TR, Cleverly J, Collalti A, Consalvo C, Cook BD, Cook D, Coursolle C, Cremonese E, Curtis PS, D'Andrea E, da Rocha H, Dai X, Davis KJ, De Cinti B, de Grandcourt A, De Ligne A, De Oliveira RC, Delpierre N, Desai AR, Di Bella CM, di Tommasi P, Dolman H, Domingo F, Dong G, Dore S, Duce P, Dufrêne E, Dunn A, Dušek J, Eamus D, Eichelmann U, ElKhidir HAM, Eugster W, Ewenz CM, Ewers B, Famulari D, Fares S, Feigenwinter I, Feitz A, Fensholt R, Filippa G, Fischer M, Frank J, Galvagno M, Gharun M, Gianelle D, Gielen B, Gioli B, Gitelson A, Goded I, Goeckede M, Goldstein AH, Gough CM, Goulden ML, Graf A, Griebel A, Gruening C, Grünwald T, Hammerle A, Han S, Han X, Hansen BU, Hanson C, Hatakka J, He Y, Hehn M,

Heinesch B, Hinko-Najera N, Hörtnagl L, Hutley L, Ibrom A, Ikawa H, Jackowicz-Korczynski M, Janouš D, Jans W, Jassal R, Jiang S, Kato T, Khomik M, Klatt J, Knohl A, Knox S, Kobayashi H, Koerber G, Kolle O, Kosugi Y, Kotani A, Kowalski A, Kruijt B, Kurbatova J, Kutsch WL, Kwon H, Launiainen S, Laurila T, Law B, Leuning R, Li Y, Liddell M, Limousin J-M, Lion M, Liska AJ, Lohila A, López-Ballesteros A, López-Blanco E, Loubet B, Loustau D, Lucas-Moffat A, Lüers J, Ma S, Macfarlane C, Magliulo V, Maier R, Mammarella I, Manca G, Marcolla B, Margolis HA, Marras S, Massman W, Mastepanov M, Matamala R, Matthes JH, Mazzenga F, McCaughey H, McHugh I, McMillan AMS, Merbold L, Meyer W, Meyers T, Miller SD, Minerbi S, Moderow U, Monson RK, Montagnani L, Moore CE, Moors E, Moreaux V, Moureaux C, Munger JW, Nakai T, Neirynck J, Nesic Z, Nicolini G, Noormets A, Northwood M, Nosetto M, Nouvellon Y, Novick K, Oechel W, Olesen JE, Ourcival J-M, Papuga SA, Parmentier F-J, Paul-Limoges E, Pavelka M, Peichl M, Pendall E, Phillips RP, Pilegaard K, Pirk N, Posse G, Powell T, Prasse H, Prober SM, Rambal S, Rannik Ü, Raz-Yaseef N, Reed D, de Dios VR, Restrepo-Coupe N, Reverter BR, Roland M, Sabbatini S, Sachs T, Saleska SR, Sánchez-Cañete EP, Sanchez-Mejia ZM, Schmid HP, Schmidt M, Schneider K, Schrader F, Schroder I, Scott RL, Sedlák P, Serrano-Ortíz P, Shao C, Shi P, Shironya I, Siebicke L, Šigut L, Silberstein R, Sirca C, Spano D, Steinbrecher R, Stevens RM, Sturtevant C, Suyker A, Tagesson T, Takanashi S, Tang Y, Tapper N, Thom J, Tiedemann F, Tomassucci M, Tuovinen J-P, Urbanski S, Valentini R, van der Molen M, van Gorsel E, van Huissteden K, Varlagin A, Verfaillie J, Vesala T, Vincke C, Vitale D, Vygodskaya N, Walker JP, Walter-Shea E, Wang H, Weber R, Westermann S, Wille C, Wofsy S, Wohlfahrt G, Wolf S, Woodgate W, Li Y, Zampedri R, Zhang J, Zhou G, Zona D, Agarwal D, Biraud S, Torn M, Papale D. 2020. The FLUXNET2015 dataset and the ONEFlux processing pipeline for eddy covariance data. Scientific Data 7:225. DOI: 10.1038/s41597-020-0534-3.

References

Draper, C. S., and R. H. Reichle (2019), Assimilation of satellite soil moisture for improved atmospheric reanalyses. *Mon. Wea. Rev.*, in press, doi:10.1175/MWR-D-18-0393.

De Jeu, R. A. M., Holmes, T. R. H., Parinussa, R. M. & Owe, M. (2014). A spatially coherent global soil moisture product with improved temporal resolution. *Journal of Hydrology*, 516: 284-296.

Gao, Y., Walker, J., Allahmoradi, M., Monerris-Belda, A., Ryu, D. & Jackson, T. J. (2015). Optical Sensing of Vegetation Water Content: A Synthesis Study. *IEEE Journal of Selected Topics in Applied Earth Observations and Remote Sensing*. 8, 4, p. 1456 - 1464 9 p.

Gevaert, A. I., Parinussa, R. M., Renzullo, L. J., Van Dijk, A. I. J. M. and De Jeu, R. A. M. (2015). Spatio-temporal evaluation of resolution enhancement for passive microwave soil moisture and vegetation optical depth. *International Journal of Applied Earth Observation and Geoinformation*.

Kamble, B., Kilic, A., Hubbard, K., 2013. Estimating crop coefficients using remote sensing-based vegetation index. Remote Sens. 5 (4), 1588–1602.

Liu, Q., and Coauthors (2011). The contributions of precipitation and soil moisture observations to the skill of soil moisture estimates in a land data assimilation system. *Journal of Hydrometeorology*, 12, 750–765, doi:10.1175/JHM-D-10-05000.1.

McKenzie, N.J., D.W. Jacquier, L.J. Ashton and H.P. Cresswell (2000), "Estimation of soil properties using the Atlas of Australian Soils," *CSIRO Land and Water Technical Report* 11/00.

Parinussa, R. M., Yilmaz, M. T., Anderson, M. C., Hain, C. R. & De Jeu, R. A. M. (2014) An intercomparison of remotely sensed soil moisture products at various spatial scales over the Iberian Peninsula. *Hydrological Processes*, 28: 4865-4876.

Park, J., Baik, J., & Choi, M. (2017). Satellite-based crop coefficient and evapotranspiration using surface soil moisture and vegetation indices in Northeast Asia. Catena, 156, 305-314

Rudiger, C., Walker, J.P., Kerr, Y.H. (2011) On The Airborne Spatial Coverage Requirement for Microwave Satellite Validation. *IEEE Geoscience and Remote Sensing Letters*, 8(4):824-828. doi:10.1109/LGRS.2011.2116766.

Santi, E. (2010). An application of the SFIM technique to enhance the spatial resolution of spaceborne microwave radiometers. *International Journal of Remote Sensing*, 31: 2419-2428.

Trout T.J., Johnson L.F. 2007 Estimating crop water use from remotely sensed NDVI, Crop Models and Reference ET. USCID Fourth International Conference on Irrigation and Drainage, The Role of Irrigation and Drainage in a sustainable Future, Eds. Clemmens, A.J., Anderson, S.S., Sacramento, California, October 3-6, 2007.

T. Mo, B. J. Choudhury, T. J. Schmugge, J. R. Wang, T. J. Jackson, "A model for the microwave emission of vegetation-covered fields", *J. Geophys. Res.*, vol. 87, no. 11, pp. 229-237, Dec. 1982.

Yee, M., Walker, J. P., Monerris, A., Rudiger, C. and Jackson, T. J. (2016). On the identification of representative in situ soil moisture monitoring stations for the validation of SMAP soil moisture products in Australia. *Journal of Hydrology*, 537,, 367-381. doi:10.1016/j.jhydrol.2016.03.060

Yee, M., Walker, J. P., Rüudiger, C., Robert M. Parinussa, Kerr, Y. and Koike, T. (2016). A comparison of SMOS and AMSR2 soil moisture using representative sites of the OzNet monitoring network. *Remote Sensing of Environment*. Manuscript in review.

Validation of GCOM-W1 products using global water and energy balance monitoring at the Murray-Darling Basin in Australia

MONASH University
Engineering